Second-order Taylor Stability Analysis of Isolated Kinematic Singularities of Closed-chain Mechanisms

Adrián Peidró, Óscar Reinoso, Arturo Gil, José María Marín, Luis Payá and Yerai Berenguer
Systems Engineering and Automation Department, Miguel Hernández University, 03202, Elche, Spain

Keywords: Closed-chain Mechanism, Isolated Singularity, Taylor Expansion, Stability.

Abstract: When the geometric design of a closed-chain mechanism is non-generic, the singularity locus of the mechanism may exhibit isolated points. It is well known that these isolated points are unstable since they disappear or generate/reveal cusps when the geometric design of the mechanism slightly deviates from a non-generic design, possibly affecting the ability of the mechanism to reconfigure without crossing undesirable singularities. This paper presents a method based on second-order Taylor expansions to determine how these isolated singularities transform when perturbing the different geometric parameters of a non-generic mechanism. The method consists in approximating the singularity locus by a conic section near the isolated singularity, and classifying the resulting conic in terms of the perturbations of the different geometric parameters. Two non-generic closed-chain mechanisms are used to illustrate the presented method: an orthogonal 3R serial arm with specified position for its tip, and the planar Stewart parallel platform.

1 INTRODUCTION

This paper presents a method based on second-order Taylor expansions to study the stability of isolated kinematic singularities in closed-chain mechanisms. Isolated singularities are a type of higher-order kinematic singularities of closed-chain mechanisms which have an important impact on the kinematics of these mechanisms. Their importance is due to the fact that these isolated singularities are related to the ability of the mechanism to reconfigure itself to attain a larger operational space without crossing undesirable singular configurations, at which the kinetostatic properties of the mechanism suffer important changes.

The problem studied in this paper is formulated next, based on the formulation introduced in (Thomas and Wenger, 2011). First, consider a closed-chain mechanism with 2 degrees of freedom (DOF). This is the usual practice when studying the singularities of closed-chain mechanisms, since this allows us to visualize and analyze the singularity locus of the mechanism in a plane, which is simpler and more intuitive. If the mechanism to be studied has more than two degrees of freedom, then one only needs to lock all the degrees of freedom except for two and/or analyze only an independent 2-DOF sub-mechanism of the complete mechanism (Thomas and Wenger, 2011; Caro et al., 2012).

Consider two kinematic variables $\mathbf{x} = [x_1, x_2]^T$ of this 2-DOF closed-chain mechanism as inputs, and other two kinematic variables $\mathbf{y} = [y_1, y_2]^T$ as outputs. These inputs and outputs can be variables defining the relative position and/or orientation between two links of interest of the considered mechanism. The choice of input and output variables depends on the type of problem to analyze (e.g., the forward or inverse kinematic problem of the mechanism). Assume that, due to the geometric and assembly constraints of the mechanism, $\mathbf{x}$ and $\mathbf{y}$ are related by the following system of two scalar input-output equations:

$$f_1(\mathbf{x}, \mathbf{y}) = 0 \quad \text{AND} \quad f_2(\mathbf{x}, \mathbf{y}) = 0 \qquad (1)$$

where f_1 and f_2 are *constraint functions*. In this paper, we define the Finite Displacement Problem (FDP) as the problem consisting in solving the outputs $\mathbf{y}$ from Eq. (1) for given inputs $\mathbf{x}$. In general, the FDP has many different solutions for the same inputs $\mathbf{x}$, i.e.:

$$\text{FDP: } \mathbf{x} \rightarrow \boxed{\text{Solve } \mathbf{y} \text{ from Eq. (1)}} \rightarrow \{\mathbf{y}^1, \ldots, \mathbf{y}^m\}$$

where m is the number of different solutions. As in (Thomas and Wenger, 2011), in this paper we will refer to the different solutions of the FDP (for a given input $\mathbf{x}$) as *assembly modes*.

This paper focuses on the singularities of the FDP, which are the configurations at which $\det(\mathbf{J}) = 0$, where $\mathbf{J} = \{j_{pq}\}$ is the 2×2 Jacobian matrix of

Peidró, A., Reinoso, Ó., Gil, A., Marín, J., Payá, L. and Berenguer, Y.
Second-order Taylor Stability Analysis of Isolated Kinematic Singularities of Closed-chain Mechanisms.
DOI: 10.5220/0006428503510358
In *Proceedings of the 14th International Conference on Informatics in Control, Automation and Robotics (ICINCO 2017) - Volume 2*, pages 351-358
ISBN: Not Available

derivatives of $\{f_1, f_2\}$ with respect to the outputs: $j_{pq} = \frac{\partial f_p}{\partial y_q}$ $(p,q \in \{1,2\})$. The condition $\det(\mathbf{J}) = 0$ defines the singularity locus of the mechanism. The singularity locus can be represented both in the input plane (x_1-x_2) and in the output plane (y_1-y_2), obtaining the singularity curves in these planes. When approaching these singularity curves in the input plane, at least two different assembly modes $\mathbf{y}^a$ and $\mathbf{y}^b$ ($a \neq b$) coalesce. When the mechanism crosses a singular configuration, it suffers a loss of dexterity or control (depending on the nature of the chosen inputs).

In this paper, we are interested in analyzing the stability of isolated points of the singularity curves (isolated singularities). When the geometric design of a closed-chain mechanism satisfies some very specific conditions (which depend on the particular topology of the mechanism), it is said that the geometry of the mechanism is *non-generic* and, in that case, the singularity curves of the mechanism exhibit isolated points [or other higher-order singularities (Thomas and Wenger, 2011)]. These isolated points are unstable, since if the geometry of the mechanism slightly deviates from the non-generic design (e.g., due to finite precision in the manufacturing of the mechanism, which impedes building it with an *exact* non-generic geometry), these isolated points disappear or transform into closed curves with cusps (Thomas and Wenger, 2011; Coste et al., 2016; Coste et al., 2013).

As it is well known, when describing closed trajectories that enclose these cusps in the input plane, the mechanism can change its assembly mode without crossing singularities (Zein et al., 2008; Husty et al., 2014; DallaLibera and Ishiguro, 2014; Peidró et al., 2015; Husty, 2009). This is beneficial to enlarge the range of operation of the mechanism without significantly affecting its kinetostatic properties, i.e., without suffering losses of dexterity or control.

Perturbing the geometry of a non-generic mechanism can importantly alter its kinematic properties. For example, if the perturbation of the non-generic geometry of the mechanism transforms an isolated singularity into a cusped closed curve, then these cusps will allow the mechanism to change its assembly mode without crossing singularities. If, on the contrary, the perturbation destroys the isolated point, then the mechanism will lose such ability to reconfigure its assembly mode. Therefore, it is important to know how the isolated singularities will transform when the geometry of a non-generic closed-chain mechanism is perturbed.

This paper presents a method to determine how the isolated singularities of closed-chain mechanisms transform when their non-generic geometry is slightly perturbed. To this end (Section 2), the singularity locus of the mechanism is approximated near the isolated singularity by its second-order Taylor expansion, which is equivalent to approximating the singularity locus by a conic section. Then, the stability analysis of the isolated singularity reduces to classifying that conic in terms of the perturbations of the different geometric parameters of the mechanism. The presented method is illustrated with two different closed-chain mechanisms in Sections 3 and 4. Finally, Section 5 presents the conclusions and future work.

2 STABILITY ANALYSIS THROUGH SECOND-ORDER TAYLOR EXPANSION

This section presents a method to study the stability of isolated kinematic singularities based on a second-order Taylor expansion. Assume that the singularity locus in the output plane (y_1-y_2) is defined by the following equation:

$$S(\mathbf{y}, \mathbf{g}) = 0 \tag{2}$$

where $S(\mathbf{y}, \mathbf{g}) = \det(\mathbf{J})$. For a given geometry $\mathbf{g} = [g_1, \ldots, g_d]^T$ of the mechanism, the previous equation defines a set of singularity curves in the y_1-y_2 plane. The concrete shape of these curves depends on the geometry $\mathbf{g}$. Assume that, for a given non-generic geometry $\mathbf{g}_0$, the singularity curves exhibit an isolated point at $\mathbf{y}_0$. Next, S will be approximated by its second-order Taylor expansion about $(\mathbf{y}_0, \mathbf{g}_0)$:

$$\begin{aligned} S(\mathbf{y}, \mathbf{g}) \approx S(\mathbf{y}_0, \mathbf{g}_0) + \left[\frac{\partial S}{\partial \mathbf{y}}(\mathbf{y}_0, \mathbf{g}_0)\right] \Delta\mathbf{y} + \\ + \left[\frac{\partial S}{\partial \mathbf{g}}(\mathbf{y}_0, \mathbf{g}_0)\right] \Delta\mathbf{g} + \left[\Delta\mathbf{y}^T, \Delta\mathbf{g}^T\right] \frac{\mathbf{H}(\mathbf{y}_0, \mathbf{g}_0)}{2} \begin{bmatrix} \Delta\mathbf{y} \\ \Delta\mathbf{g} \end{bmatrix} \end{aligned} \tag{3}$$

where $\mathbf{H}$ is the (symmetric) Hessian matrix of S with respect to $\mathbf{y}$ and $\mathbf{g}$, $\Delta\mathbf{y} = \mathbf{y} - \mathbf{y}_0$ and $\Delta\mathbf{g} = \mathbf{g} - \mathbf{g}_0$. Note that $S(\mathbf{y}_0, \mathbf{g}_0) = 0$ because the point $\mathbf{y}_0$ belongs to the singularity curves corresponding to the geometry $\mathbf{g}_0$. Moreover, since $\mathbf{y}_0$ is an isolated point (thus, a critical or special point) of these curves, then:

$$\frac{\partial S}{\partial \mathbf{y}}(\mathbf{y}_0, \mathbf{g}_0) = [0, 0] \tag{4}$$

which justifies the need for a second-order expansion [otherwise, the following Eq. (5) would not define a curve in the output plane]. Substituting (3) into Eq. (2) yields the equation defining the singularity locus near the isolated singular point $\mathbf{y}_0$ and near $\mathbf{g}_0$:

$$\mathbf{S}_\mathbf{g}\Delta\mathbf{g} + \left[\Delta\mathbf{y}^T, \Delta\mathbf{g}^T\right] \frac{\mathbf{H}(\mathbf{y}_0, \mathbf{g}_0)}{2} \begin{bmatrix} \Delta\mathbf{y} \\ \Delta\mathbf{g} \end{bmatrix} = 0 \tag{5}$$

Table 1: DH parameters of the robot shown in Figure 1.

DH parameter →	θ	d	α	a
$0 \rightarrow 1$	ϕ_1	0	$\pi/2$	d_2
$1 \rightarrow 2$	ϕ_2	$-r_2$	$-\pi/2$	d_3
$2 \rightarrow 3$	ϕ_3	r_3	0	d_4

where $\mathbf{S_g} = \frac{\partial S}{\partial \mathbf{g}}(\mathbf{y}_0, \mathbf{g}_0)$. Next, the Hessian $\mathbf{H}$ is partitioned as follows:

$$\mathbf{H} = \begin{bmatrix} \mathbf{H}_{11} & \mathbf{H}_{12} \\ \mathbf{H}_{12}^T & \mathbf{H}_{22} \end{bmatrix} \tag{6}$$

where the sizes of $\mathbf{H}_{11}$, $\mathbf{H}_{12}$ and $\mathbf{H}_{22}$ are 2×2, $2\times d$ and $d\times d$, respectively. Using this partition of $\mathbf{H}$, Eq. (5) can be rewritten as follows:

$$[\Delta\mathbf{y}^T, 1] \underbrace{\begin{bmatrix} \mathbf{H}_{11}/2 & \mathbf{K} \\ \mathbf{K}^T & u \end{bmatrix}}_{\mathbf{C}} \begin{bmatrix} \Delta\mathbf{y} \\ 1 \end{bmatrix} = 0 \tag{7}$$

where:

$$\mathbf{K} = \frac{\mathbf{H}_{12}\Delta\mathbf{g}}{2} \quad \text{and} \quad u = \left(\Delta\mathbf{g}^T \frac{\mathbf{H}_{22}}{2} + \mathbf{S_g}\right)\Delta\mathbf{g} \tag{8}$$

Equation (7) defines a conic in the output plane y_1-y_2. The type of conic defined depends on the coefficient matrix $\mathbf{C}$ (Srinivasan, 2003). Note that $\mathbf{C}$ depends on the perturbation $\Delta\mathbf{g}$ from the non-generic geometry $\mathbf{g}_0$. Thus, to study how the perturbations in the geometry of the robot affect the stability of the isolated singularity $\mathbf{y}_0$, we only need to study and classify the type of conic defined by $\mathbf{C}$ in terms of $\Delta\mathbf{g}$.

In the next sections, we will apply this method to study the stability of isolated singularities in two closed-chain mechanisms.

3 EXAMPLE 1: ORTHOGONAL 3R SERIAL ARM

This section analyzes the stability of isolated kinematic singularities in the orthogonal 3R serial robot studied in (Thomas and Wenger, 2011). This serial robot, shown in Figure 1, has three revolute joints arranged in such a way that consecutive revolute axes are orthogonal. In this robot, the three joint angles ϕ_1, ϕ_2 and ϕ_3 (which are the rotations about the axes z_0, z_1 and z_2 of Figure 1, respectively) are used to control the position $\mathbf{p} = [p_x, p_y, p_z]^T$ of the tip.

The DH parameters of this robot are shown in Table 1, where $\mathbf{g} = [d_2, d_3, d_4, r_2, r_3]^T$ are the geometric parameters. Multiplying the corresponding DH matrices yields the position of the tip in terms of ϕ_i:

$$p_x = c_1(c_2(d_4c_3 + d_3) - r_3s_2 + d_2) - s_1(d_4s_3 + r_2) \tag{9}$$

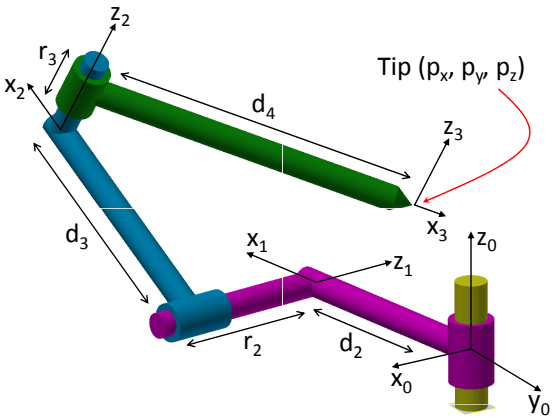

Figure 1: Orthogonal 3R serial robot studied in (Thomas and Wenger, 2011).

$$p_y = s_1(c_2(d_4c_3 + d_3) - r_3s_2 + d_2) + c_1(d_4s_3 + r_2) \tag{10}$$

$$p_z = r_3c_2 + s_2(d_4c_3 + d_3) \tag{11}$$

where $s_i = \sin\phi_i$ and $c_i = \cos\phi_i$ ($i \in \{1,2,3\}$). The position of the tip can also be given in cylindrical coordinates (ϕ, ρ, p_z) (Thomas and Wenger, 2011), where

$$\rho = \sqrt{p_x^2 + p_y^2} \tag{12}$$

is the radial coordinate, ϕ is the polar angle and p_z is the height or axial coordinate. Since ρ and p_z only depend on the joint angles ϕ_2 and ϕ_3, we can focus only on the sub-arm composed of these two joints, and consider that this 2-DOF serial sub-arm is used to control the radial and axial coordinates of the tip of the robot (Thomas and Wenger, 2011).

Although this 2-DOF sub-arm is a serial robot (i.e., with open architecture), specifying the cylindrical coordinates (ρ, p_z) of its tip transforms it into a 2-DOF closed-loop mechanism in which the inputs are the specified radial and axial coordinates of the tip ($\mathbf{x} = [\rho, p_z]^T$) and the outputs are the last two joint angles ($\mathbf{y} = [\phi_2, \phi_3]^T$). Thus, the Finite Displacement Problem studied in this section coincides with the inverse kinematics of this 2-DOF serial sub-arm.

The input-output equation [Eq. (1)] of this mechanism is composed of Eqs. (11) and (12), from which the constraint functions f_1 and f_2 are identified:

$$\begin{aligned} f_1 = &-\rho^2 + c_2^2(d4^2c_3^2 + 2d_3d_4c_3 + d_3^2) \\ &- c_2(s_2(2d_4r_3c_3 + 2d_3r_3) - 2d_2d_4c_3 - 2d_2d_3) \\ &+ r_3^2s_2^2 - 2d_2r_3s_2 + d_4^2s_3^2 + 2d_4r_2s_3 + d_2^2 + r_2^2 \end{aligned} \tag{13}$$

$$f_2 = r_3c_2 + s_2(d_4c_3 + d_3) - p_z \tag{14}$$

According to Eq. (2), the singularity locus of this mechanism in the output plane is defined by:

$$S(\mathbf{y}, \mathbf{g}) = \frac{\partial f_1}{\partial \phi_2}\frac{\partial f_2}{\partial \phi_3} - \frac{\partial f_1}{\partial \phi_3}\frac{\partial f_2}{\partial \phi_2} = 0 \tag{15}$$

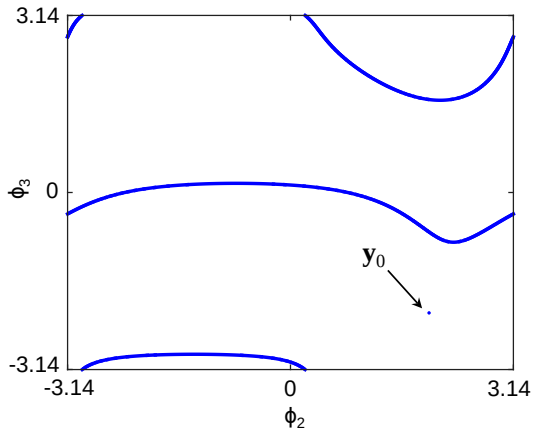

Figure 2: Singularity locus of a non-generic orthogonal 3R serial robot in the ϕ_2-ϕ_3 plane.

S only depends on the output variables $\mathbf{y} = [\phi_2, \phi_3]^T$ and on the geometric parameters $\mathbf{g}$ (the inputs disappear due to the partial derivatives). The resulting expression of $S(\mathbf{y}, \mathbf{g})$ is not shown here due to its length.

The concrete shape of the singularity curves defined by $S(\mathbf{y}, \mathbf{g}) = 0$ will depend on the value of the geometric parameters $\mathbf{g}$. Next, we will analyze one of the non-generic geometries studied in (Thomas and Wenger, 2011), defined by the following values: $\mathbf{g}_0 = [1, 0.5, 0.3327820876, 0.2, 0.8]^T$. For this geometry, the singularity curves exhibit an isolated point $\mathbf{y}_0 = [1.953146918, -2.13618956]^T$ rad (see Figure 2). As it is well known (Thomas and Wenger, 2011), this isolated point is a higher-order unstable singularity [called *lips* when represented in the ρ-p_z plane using Eqs. (12) and (11)], for if the geometry of the robot slightly deviates from the non-generic geometry $\mathbf{g}_0$, then the isolated point $\mathbf{y}_0$ transforms into a loop or even disappears, possibly altering the kinematic properties of the mechanism. Applying the analysis presented in Section 2 will allow us to determine how $\mathbf{y}_0$ transforms depending on how the geometry of the mechanism is perturbed away from $\mathbf{g}_0$.

Next, consider that all the geometric parameters suffer a small perturbation $\Delta\mathbf{g} = [\Delta d_2, \Delta d_3, \Delta d_4, \Delta r_2, \Delta r_3]^T$ from the non-generic geometry $\mathbf{g}_0$ indicated in the previous paragraph. Substituting $\mathbf{y}_0$ and $\mathbf{g}_0$ into Eq. (7) yields the equation of a conic curve that approximates the perturbed singularity locus in the output plane ϕ_2-ϕ_3, where:

$$\frac{\mathbf{H}_{11}}{2} = \begin{bmatrix} -0.0904 & 0.0273 \\ 0.0273 & -0.1128 \end{bmatrix} \tag{16}$$

$$\mathbf{K} = \begin{bmatrix} 0 & -0.1362 \\ 0.09725 & 0.05913 \\ -0.05211 & -0.1376 \\ -1.760 \cdot 10^{-10} & 0.2235 \\ -0.03911 & 0.1348 \end{bmatrix}^T \Delta\mathbf{g} \tag{17}$$

$$\begin{aligned} u = &-0.5616\Delta d_2\Delta d_3 - 0.242\Delta d_2\Delta d_4 - 0.1807\Delta d_2 \\ &+ 0.2096\Delta d_3^2 - 0.1097\Delta d_3\Delta d_4 - 0.1328\Delta d_3\Delta r_2 \\ &+ 0.5209\Delta d_3\Delta r_3 + 0.0008248\Delta d_3 + 0.7776\Delta d_4^2 \\ &- 0.8519\Delta d_4\Delta r_2 + 0.584\Delta d_4\Delta r_3 + 0.2589\Delta d_4 \\ &- 0.3303\Delta r_2\Delta r_3 - 0.3069\Delta r_2 + 0.1941\Delta r_3 \end{aligned} \tag{18}$$

The type of conic defined by Eq. (7) depends on $\mathbf{H}_{11}$, $\mathbf{K}$ and u (Srinivasan, 2003). First, since $\det(\mathbf{H}_{11}) > 0$, then the perturbed singularity locus is an ellipse (either real or imaginary). The type of ellipse defined by Eq. (7) depends on $\omega = c_{11}\det(\mathbf{C})$, where c_{11} is the first element of the first row of $\mathbf{C}$:

- If $\omega > 0$, then Eq. (7) defines an imaginary ellipse.
- If $\omega < 0$, then Eq. (7) defines a real ellipse.

If $\omega = 0$, then the ellipse degenerates into a single point. The perturbation $\Delta\mathbf{g}$ of the geometric parameters will determine the sign of ω and, therefore, will determine the type of ellipse into which the isolated point $\mathbf{y}_0$ transforms when the geometry of the robot slightly deviates from the non-generic geometry $\mathbf{g}_0$.

3.1 Perturbing One Geometric Parameter

For simplicity, consider first that only d_4 is perturbed, i.e., $\Delta\mathbf{g} = [0, 0, \Delta d_4, 0, 0]^T$ [this is the situation studied in (Thomas and Wenger, 2011)]. In that case:

$$\omega = -(0.0008835\Delta d_4 + 0.0002213)\Delta d_4 \tag{19}$$

By plotting Eq. (19) (see Figure 3), we can identify three cases for small perturbations Δd_4:

- If $\Delta d_4 > 0$, then $\omega < 0 \rightarrow$ the singularity locus is a real ellipse.
- If $\Delta d_4 < 0$, then $\omega > 0 \rightarrow$ the singularity locus is an imaginary ellipse
- If $\Delta d_4 = 0$, then $\omega = 0 \rightarrow$ the singularity locus is a (real) ellipse shrunk into a point.

Thus, if d_4 is slightly increased from its non-generic value ($\Delta d_4 > 0$), the isolated point $\mathbf{y}_0$ transforms into a tiny real ellipse E_r in the ϕ_2-ϕ_3 plane. As Δd_4 decreases and approaches zero, the size of this real ellipse continuously decreases, until it shrinks into the point $\mathbf{y}_0$ when $\Delta d_4 = 0$ (i.e., the isolated point $\mathbf{y}_0$ remains unaltered since the non-generic geometry of the mechanism is not altered). If the perturbation is further decreased and becomes negative ($\Delta d_4 < 0$), then the point $\mathbf{y}_0$ transforms into an imaginary ellipse, i.e., $\mathbf{y}_0$ disappears from the (real) ϕ_2-ϕ_3 plane.

Figure 4a illustrates the transformation of $\mathbf{y}_0$ into an approximately elliptic loop E_r for $\Delta d_4 = 0.0002$: the ellipse defined by Eq. (7) is represented in green

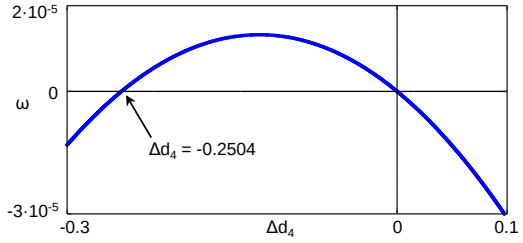

Figure 3: Variation of ω with Δd_4.

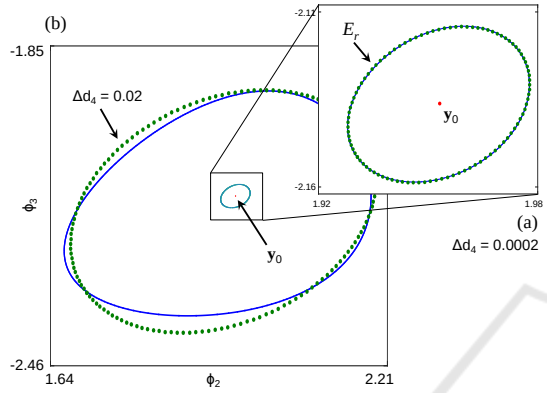

Figure 4: Transformation of the singularity locus near $\mathbf{y}_0$ into an approximately elliptic loop when perturbing d_4.

dotted line, whereas the exact singularity locus [defined by Eq. (15)] is represented in blue continuous line. Note that Eq. (7) approximates the exact singularity locus very accurately for small perturbations, but for large perturbations this approximation is not valid (e.g., see Figure 4b, where $\Delta d_4 = 0.02$).

If the real ellipse E_r is mapped to the input plane using Eqs. (11) and (12), then it transforms into a small closed curve with two cusps (see Figure 5). It is well known that these cusps allow the mechanism to reconfigure between different assembly modes without crossing singularities. Thus, the destruction of the real ellipse corresponds to the destruction of these two cusps and, therefore, the mechanism loses such ability to reconfigure without crossing singularities.

The previous results regarding the relationship between the sign of Δd_4 and the stability of the isolated point $\mathbf{y}_0$, obtained by analyzing the sign of ω in Eq. (19), agree with (Thomas and Wenger, 2011), where the singularity locus was plotted in the ρ-p_z plane for different values of d_4 both above and below the non-generic geometry ($d_4 = 0.3327820876$).

Note that, according to Figure 3, ω becomes again negative for $\Delta d_4 < -0.2504$, which means that the real ellipse E_r defined by Eq. (7) reappears again for $\Delta d_4 < -0.2504$. This may erroneously suggest that the exact singularity locus, defined by Eq. (15), should also exhibit a small loop due to the reappearance of the ellipse E_r. However, this is not true because the perturbation $\Delta d_4 = -0.2504$ is too large for Eq. (7) to be a valid approximation of the exact singularity locus. Thus, the analysis of the sign of ω in Eq. (19) is only valid for sufficiently small values of $|\Delta d_4|$. It can be checked that, unlike in Figure 4, the exact singularity locus does not exhibit small (approximately elliptic) loops for $\Delta d_4 < -0.2504$.

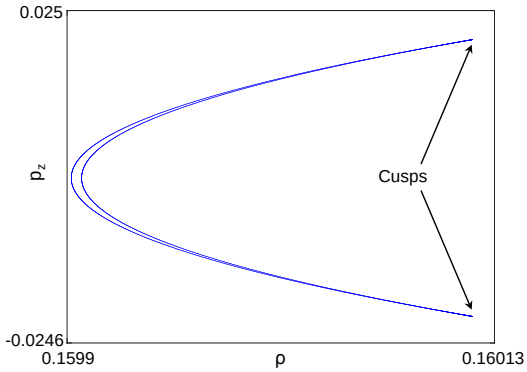

Figure 5: Closed curve with two cusps at ($\rho \approx 0.16012, p_z \approx \pm 0.020653$), obtained as the image of the ellipse E_r of Figure 4a in the ρ-p_z plane.

3.2 Perturbing Two Geometric Parameters

Next, consider that both d_4 and r_2 are perturbed from the non-generic geometry $\mathbf{g}_0$, i.e.: $\Delta\mathbf{g} = [0,0,\Delta d_4,\Delta r_2,0]^T$. In that case, ω equals:

$$\omega = -0.0008835\Delta d_4^2 + 0.001289\Delta d_4\Delta r_2 - 0.0002213\Delta d_4 - 0.0004083\Delta r_2^2 + 0.0002625\Delta r_2 \quad (20)$$

Figure 6 shows how the sign of ω depends on the perturbations Δd_4 and Δr_2. The Δd_4-Δr_2 plane is divided into three regions $\{R_1, R_2, R_3\}$ by the hyperbola with branches $\{h_1, h_2\}$, which is defined by $\omega = 0$. Since $\omega < 0$ in region R_1, then Eq. (7) defines a real ellipse for perturbations falling in that region. This means that, for perturbations in region R_1, the isolated point $\mathbf{y}_0$ deforms into a small (approximately elliptic) loop in the output plane. This loop transforms into a closed curve with two cusps when mapped to the input plane using Eqs. (12) and (11). Figure 7 shows an example of this, for the following perturbation (which falls in region R_1): $\Delta d_4 = 0.0002$, $\Delta r_2 = -0.0002$.

For perturbations falling in R_2, we have $\omega > 0$ and, therefore, Eq. (7) defines an imaginary ellipse. This means that the point $\mathbf{y}_0$ disappears for perturbations belonging to region R_2, and the mechanism loses the

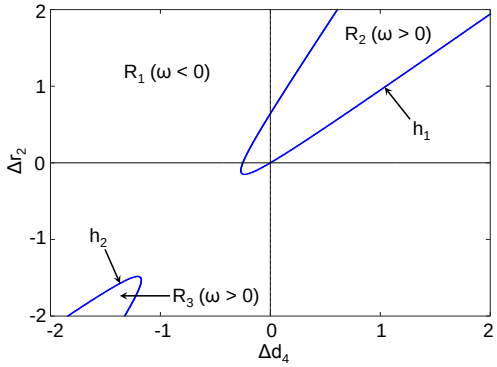

Figure 6: Variation of the sign of ω [Eq. (20)] with the perturbations Δd_4 and Δr_2.

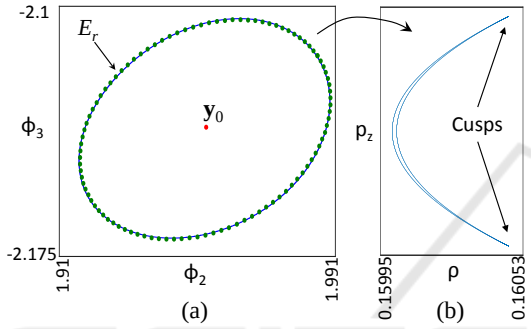

Figure 7: (a) An (approximately) elliptic loop E_r of the singularity locus of a perturbed orthogonal 3R serial robot. (b) Image of E_r in the input plane, which presents two cusps at $(\rho \approx 0.16047, p_z \approx \pm 0.03051)$.

ability to change between different solutions of the FDP without crossing singularities.

Finally, it is important to remark again that the behavior of the exact singularity locus [defined by Eq. (15)] under large perturbations cannot be predicted by analyzing the transformations suffered by the ellipse defined by Eq. (7). For example, according to Figure 6, the nature of the ellipse defined by Eq. (7) changes between real and imaginary when crossing the branch h_2 of the hyperbola $\omega = 0$ (i.e., when both perturbations Δd_4 and Δr_2 are sufficiently negative). This does not mean that the exact singularity locus of the mechanism loses an (approximately) elliptic loop when passing from region R_1 to region R_3, because h_2 is crossed for perturbations so large that render the quadratic approximation of Eq. (7) invalid.

4 EXAMPLE 2: PLANAR STEWART PLATFORM

In this section, the proposed method will be used to analyze the stability of the isolated singularities of

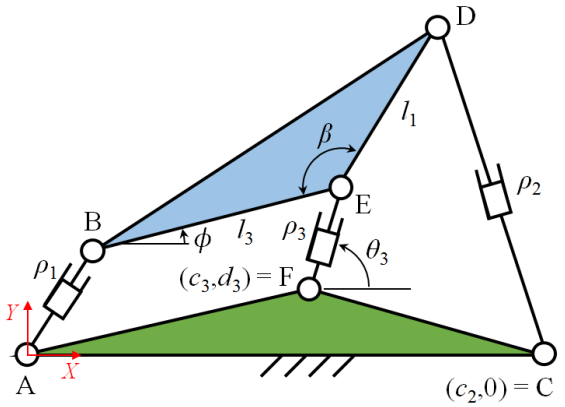

Figure 8: General 3RPR planar parallel robot.

the planar Stewart platform. Consider first a general 3RPR planar parallel robot (Figure 8), which is composed of a fixed base AFC and a mobile platform BDE interconnected by three actuated prismatic limbs (P) through revolute joints (R). In this robot, three linear actuators {AB,CD,EF}, with respective lengths $\{\rho_1,\rho_2,\rho_3\}$, are used to control the position and orientation of the triangular platform BDE. The position of the mobile platform can be parameterized by the polar coordinates (ρ_3, θ_3) of joint E, whereas its orientation can be parameterized by the angle ϕ.

To apply the method described in Section 2, we need a 2-DOF closed-chain mechanism. Therefore, from now on, the prismatic joint of the limb EF will be locked, and its length ρ_3 will be assumed to be constant. In this way, we will deal with a 2-DOF closed-chain mechanism with inputs $\mathbf{x} = [\rho_1, \rho_2]^T$ and outputs $\mathbf{y} = [\theta_3, \phi]^T$. All the remaining parameters indicated in Figure 8 will be considered as geometric design parameters, i.e., $\mathbf{g} = [c_2, c_3, d_3, l_1, l_3, \beta, \rho_3]^T$. For this mechanism, the input-output equations (1) are obtained by imposing the condition that the lengths of the limbs AB and CD should be ρ_1 and ρ_2, respectively. This yields the following constraint functions:

$$\begin{aligned} f_1 = &-2l_3\rho_3 c_{\theta_3} c_\phi + 2c_3\rho_3 c_{\theta_3} - 2l_3\rho_3 s_{\theta_3} s_\phi \\ &+ 2d_3\rho_3 s_{\theta_3} - 2c_3 l_3 c_\phi - 2d_3 l_3 s_\phi \\ &+ c_3^2 + d_3^2 + l_3^2 + \rho_3^2 - \rho_1^2 \end{aligned} \quad (21)$$

$$\begin{aligned} f_2 = &-2l_1\rho_3 c_\beta c_{\theta_3} c_\phi - 2l_1\rho_3 c_\beta s_{\theta_3} s_\phi + 2c_2 l_1 c_\beta c_\phi \\ &- 2c_3 l_1 c_\beta c_\phi - 2d_3 l_1 c_\beta s_\phi - 2l_1\rho_3 s_\beta c_{\theta_3} s_\phi \\ &+ 2l_1\rho_3 s_\beta s_{\theta_3} c_\phi + 2d_3 l_1 s_\beta c_\phi + 2c_2 l_1 s_\beta s_\phi \\ &- 2c_3 l_1 s_\beta s_\phi - 2c_2\rho_3 c_{\theta_3} + 2c_3\rho_3 c_{\theta_3} \\ &+ 2d_3\rho_3 s_{\theta_3} + c_2^2 - 2c_2 c_3 + c_3^2 \\ &+ d_3^2 + l_1^2 + \rho_3^2 - \rho_2^2 \end{aligned} \quad (22)$$

where $s_w = \sin w$ and $c_w = \cos w$ $(w \in \{\beta, \phi, \theta_3\})$. The singularity locus of this mechanism in the output

plane is defined by the following equation:

$$S(\mathbf{y},\mathbf{g}) = \frac{\partial f_1}{\partial \theta_3}\frac{\partial f_2}{\partial \phi} - \frac{\partial f_1}{\partial \phi}\frac{\partial f_2}{\partial \theta_3} = 0 \qquad (23)$$

Equation (23) does not depend on the inputs because they vanish due to the partial derivatives. The shape of the singularity locus depends on the value of the geometric design parameters $\mathbf{g}$. In the following, we will analyze the singularity locus of the non-generic geometry analyzed in (Peidró et al., 2016). The considered non-generic geometry is defined by $\mathbf{g}_0 = [1.5, 0.5, 0, 0.5, 0.5, \pi \text{ rad}, 1]^T$. This geometric design is non-generic because it implies that the three joints AFC of the base are perfectly aligned ($d_3 = 0$), and also that the three joints BDE of the mobile platform are perfectly aligned ($\beta = \pi$ rad). This design of the 3RPR parallel robot can be considered as a planar version of the Stewart platform (Haug et al., 1995).

Figure 9 shows the singularity locus in the output plane corresponding to the considered non-generic geometry $\mathbf{g}_0$. This singularity locus exhibits an isolated point at $\mathbf{y}_0 = [\pi, 0]$ rad. Next, we will apply the analysis of Section 2 to analyze the stability of this isolated point. Consider that all the geometric parameters suffer a small deviation from $\mathbf{g}_0$, i.e.: $\Delta\mathbf{g} = [\Delta c_2, \Delta c_3, \Delta d_3, \Delta l_1, \Delta l_3, \Delta\beta, \Delta\rho_3]^T$. Substituting $\mathbf{y}_0$ and $\mathbf{g}_0$ into Eq. (7), which approximates the singularity locus in the output plane near $\mathbf{y}_0$, yields:

$$\frac{\mathbf{H}_{11}}{2} = \begin{bmatrix} 1 & -0.25 \\ -0.25 & 1.5 \end{bmatrix} \qquad (24)$$

$$\mathbf{K} = [1.5\Delta d_3 - 0.5\Delta\beta, -2.5\Delta d_3 - 0.75\Delta\beta]^T \qquad (25)$$

$$u = 5\Delta d_3\Delta\beta - 4\Delta d_3^2 \qquad (26)$$

Although all the geometric parameters are perturbed, according to Eqs. (25) and (26), the transformation of $\mathbf{y}_0$ depends only on the perturbations of d_3 and β, which are precisely the only two geometric parameters that determine whether $\mathbf{g}_0$ is a generic geometry or not (since these two parameters determine if the base and platform joints are respectively aligned). In the example of Section 3, the transformation of the isolated singularity depended on the perturbations of all the geometric parameters [see Eqs. (17) and (18)].

Since $\det(\mathbf{H}_{11}) > 0$, Eq. (7) defines a real or imaginary ellipse, depending on the sign of $\omega = c_{11}\det(\mathbf{C})$:

$$\omega = -1.125(12\Delta d_3^2 - 5\Delta d_3\Delta\beta + \Delta\beta^2) \qquad (27)$$

ω in Eq. (27) is a negative definite quadratic form, i.e., $\omega < 0\ \forall(\Delta d_3, \Delta\beta) \neq (0,0)$. Therefore, if any of the two geometric parameters $\{d_3, \beta\}$ deviates from its non-generic value, then Eq. (7) defines a real ellipse in the output plane, independently of the direction of these perturbations. This means that the isolated point

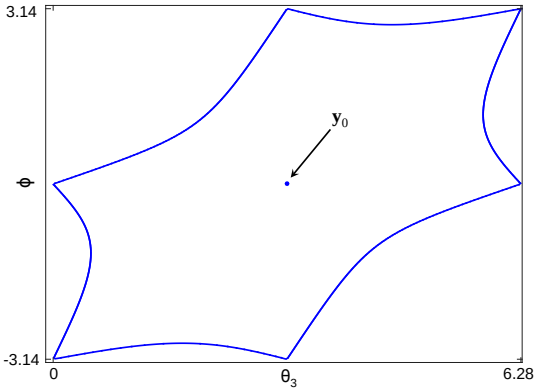

Figure 9: Singularity locus of a planar Stewart platform.

$\mathbf{y}_0$ of the exact singularity locus always deforms into a small loop that can be approximated by an ellipse if the perturbations are sufficiently small.

If this ellipse is mapped to the input plane, then it transforms into a deltoid δ, which is a closed curve with three cusp points (see the example of Figure 10). This deltoid is very important for the kinematics of the mechanism, since varying the inputs along a closed trajectory that encloses any of these individual cusps allows the mechanism to switch between different assembly modes. Encircling the whole deltoid (i.e., the three cusps simultaneously) also has this effect (Coste et al., 2016; Peidró et al., 2016).

In (Peidró et al., 2016), the following analysis was presented: departing from the non-generic geometry $\mathbf{g}_0$ analyzed in this section, the geometric parameters d_3 and β were numerically perturbed to study how the mentioned deltoid δ was affected by these perturbations. That analysis showed that the shape and size of the deltoid δ vary due to these perturbations, and it degenerates into a point (which is the image of $\mathbf{y}_0$ in the input plane) when the perturbations tend to zero. However, no perturbation could be found in (Peidró et al., 2016) that destroys the deltoid δ in the same way that the bicuspidal closed curve of Figure 5 can be destroyed by rendering the ellipse E_r (which generates this bicuspidal curve) imaginary ($\omega > 0$). This is because a deltoid is a stable singularity obtained when perturbing a singularity of multiplicity 4, which is the case of the isolated point $\mathbf{y}_0$ (Coste et al., 2016).

In this aspect, the analysis presented in this section complements the analysis presented in (Peidró et al., 2016) and illustrates the fact that the deltoid δ cannot be destroyed by any combination of perturbations from the non-generic geometry $\mathbf{g}_0$: in the analyzed 3RPR robot, these perturbations *always* transform the isolated point $\mathbf{y}_0$ into a real ellipse, and the image of this real ellipse in the input plane is the deltoid δ.

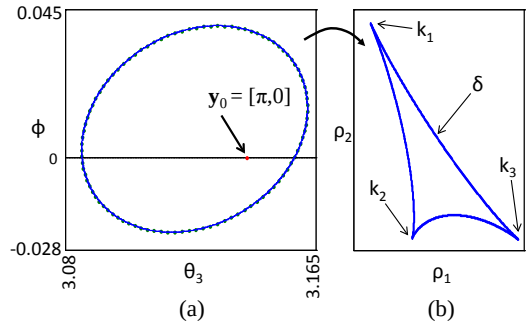

Figure 10: (a) (Approximately elliptic) singularity locus near $\mathbf{y}_0$ when the non-generic geometry of a planar Stewart platform is slightly perturbed ($\Delta d_3 = 0.01$, $\Delta\beta = -0.01$). (b) The image of this ellipse in the input plane is a deltoid δ, with cusps: $k_1 \approx (0.9995, 1.5014)$, $k_2 \approx (0.9999, 1.4999)$ and $k_3 \approx (1.0009, 1.4999)$.

5 CONCLUSION

This paper has presented a method to determine how isolated singularities of closed-chain mechanisms transform when the geometric design parameters of the mechanism slightly deviate from a non-generic design. The method consists in approximating the singularity locus by a conic section and classifying it in terms of the perturbations of the different geometric parameters of the mechanism. The method has been illustrated with two closed-chain mechanisms whose singularity loci exhibit isolated points.

In the future, we will extend this analysis to other higher-order singularities besides isolated points, and to mechanisms with more than 2 DOF. In addition, we will explore the application of the proposed method in the robust design of cuspidal parallel robots.

ACKNOWLEDGEMENTS

This work was supported by the Spanish Ministries of Education (grant number FPU13/00413) and Economy (project number DPI 2016-78361-R).

REFERENCES

Caro, S., Wenger, P., and Chablat, D. (2012). Non-singular assembly mode changing trajectories of a 6-DOF parallel robot. In *The ASME 2012 International Design Engineering Technical Conferences & Computers and Information in Engineering Conference*, pages 1–10.

Coste, M., Chablat, D., and Wenger, P. (2013). *New Trends in Mechanism and Machine Science: Theory and Applications in Engineering*, chapter Perturbation of Symmetric 3-RPR Manipulators and Asymptotic Singularities, pages 23–31. Springer Netherlands, Dordrecht.

Coste, M., Wenger, P., and Chablat, D. (2016). Hidden cusps. In *15th International Symposium on Advances in Robot Kinematics*, pages 1–9.

DallaLibera, F. and Ishiguro, H. (2014). Non-singular transitions between assembly modes of 2-DOF planar parallel manipulators with a passive leg. *Mech. Mach. Theory*, 77:182–197.

Haug, E. J., Adkins, F. A., Qiu, C. C., and Yen, J. (1995). Analysis of barriers to control of manipulators within accessible output sets. In *Proceedings of the 20th ASME Design Engineering Technical Conference*, pages 697–704.

Husty, M. (2009). Non-singular assembly mode change in 3-RPR-parallel manipulators. In Kecskeméthy, A. and Müller, A., editors, *Computational Kinematics*, pages 51–60. Springer Berlin Heidelberg.

Husty, M., Schadlbauer, J., Caro, S., and Wenger, P. (2014). The 3-RPS manipulator can have non-singular assembly-mode changes. In Thomas, F. and Pérez Gracia, A., editors, *Computational Kinematics*, volume 15 of *Mechanisms and Machine Science*, pages 339–348. Springer Netherlands.

Peidró, A., Gil, A., Marín, J. M., Payá, L., and Reinoso, Ó. (2016). On the stability of the quadruple solutions of the forward kinematic problem in analytic parallel robots. *Journal of Intelligent & Robotic Systems*, pages 1–16.

Peidró, A., Reinoso, O., Gil, A., Marín, J., and Payá, L. (2015). A virtual laboratory to simulate the control of parallel robots. *IFAC-PapersOnLine*, 48(29):19–24.

Srinivasan, V. (2003). *Theory of Dimensioning: An Introduction to Parameterizing Geometric Models*. CRC Press.

Thomas, F. and Wenger, P. (2011). On the topological characterization of robot singularity loci. a catastrophe-theoretic approach. In *Proceedings of the 2011 IEEE International Conference on Robotics and Automation*, pages 3940–3945.

Zein, M., Wenger, P., and Chablat, D. (2008). Non-singular assembly-mode changing motions for 3-RPR parallel manipulators. *Mech. Mach. Theory*, 43(4):480–490.